Check for updates

Anti-Arrhenius passage of gaseous molecules through nanoporous two-dimensional membranes

Petr Dementyev [ID] * and Armin Gölzhäuser [ID]

The passage of molecules through membranes is known to follow an Arrhenius-like kinetics, *i.e.* the flux is accelerated upon heating and *vice versa*. There exist though stepwise processes whose rates can decrease with temperature if, for example, adsorbed intermediates are involved. In this study, we perform temperature-variable permeation experiments in the range from −50 to +50 °C and observe anti-Arrhenius behaviour of water and ammonia permeating in two-dimensional freestanding carbon nanomembranes (CNMs). The permeation rate of water vapour is found to decrease many-fold with warming, while the passage of ammonia molecules strongly increases when the membrane is cooled down to the dew point. Liquefaction of isobutylene shows no enhancement for its transmembrane flux which is consistent with the material's pore architecture. The effects are described by the Clausius–Clapeyron relationship and highlight the key role of gas–surface interactions in two-dimensional membranes.

Introduction

Material transport through two-dimensional (2D) membranes is of fundamental physical interest as well as of critical importance for separation applications. Recently, an investigation of molecular movements in spatially confined nanoconduits contributed to the exploration of quantum friction, *i.e.* molecule–wall interactions at the boundary between classical and quantum mechanical behaviours.[1] In technical applications, the type of flow when molecules and atoms translocate through nanopores defines a 2D membrane's separation behaviour. Porous 2D materials have been suggested to be developed into perfect membranes and in the last decade, perforated graphene has been serving as a prototypical and frequently used 2D membrane.[2–13] Its ultimate thickness was believed to enable high-flux and high-selectivity separation and allow for distinct mass transfer behaviour.[14]

Gas permeation in 2D membranes was predicted to include a surface pathway where gaseous molecules would cross the pores in the adsorbed state.[15] This could offer additional routes to control the permselectivity; however, such a surface diffusion of adsorbates was barely observed in experiments with perforated graphene as the size distribution of its artificial pores is broad, and the permeation rate can thus be easily dominated by the gas-phase pathway across larger openings. In addition, physisorption of noble and atmospheric gases on the inert graphitic surface is unfavourable under normal conditions, and the material integrity limits the areal pore density in graphene

Physics of Supramolecular Systems and Surfaces, Bielefeld University, 33615 Bielefeld, Germany. E-mail: dementyev@physik.uni-bielefeld.de

membranes; therefore, the likelihood of adsorbed species to overcome long distances towards the defects seems to be rather small.

Unlike regular gases with low boiling points, vaporous water and organic solvents exhibit strong intermolecular interactions and readily adsorb at room temperature.[16] As prescribed by the classical adsorption isotherms, exposing flat substrates to saturated vapours results in multimolecular surface coverages.[17] Given little spacing between the openings, various 2D membranes with intrinsic microporosity were found to pass vaporous substances at high rates.[18–20] While the surface flow is accompanied by molecular effusion in pores larger than one nm, it appears to prevail at sub-nanometer dimensions. The selectivity over ordinary gases agrees with early predictions suggesting greater probability of adsorbates to permeate through nanoscale membranes.[21] In order to increase the residence time of gas particles in the vicinity of the pores, the membrane surface can be modified with ionic liquids or other chemical absorbents.[22–24] However, there is another unexplored way to impact the number of surface species according to adsorption–desorption equilibria, and that is the membrane temperature.

To identify and understand surface pathways in molecular transport through 2D membranes, we have performed temperature dependent gas permeation measurements through freestanding carbon nanomembranes (CNMs). CNMs possess a high density of sub-nanometer channels that are known to rapidly transmit water molecules.[25] We investigated the permeation of three different substances: water, ammonia, and isobutylene while the CNMs were held at temperatures between −50 °C and +50 °C. To vary the temperature, we designed a simple heat conductor that is capable of both cooling and heating the membrane in a vacuum apparatus developed

This journal is © the Owner Societies 2024

Phys. Chem. Chem. Phys., 2024, **26**, 6949–6955 | **6949**

before.[18] The transient-temperature experiments are carried out upon immersing the heat conductor into either liquid nitrogen or hot water, whereas the feed pressure is fixed. For water, we found that elevating the membrane temperature to +50 °C considerably decreases the flux which indicates that less water molecules adsorb. In turn, ammonia molecules do not permeate CNMs at room temperature. This changes drastically when the membrane temperature is lowered to −50 °C, and the relative pressure approaches saturation. We found that the onset of permeation depends on both the gas pressure and the membrane temperature reflecting a gas-to-liquid phase transition aka condensation. In the case of isobutylene, we observed no permeation in the investigated temperature range.

Experimental

The experimental system for the vapour and gas permeation measurements is based on a high-vacuum detection chamber with a quadrupole mass spectrometer (QMS) from Hiden Analytical and a feed chamber with a Baratron capacitance manometer from MKS Instruments.[18] The membrane cell separating the down- and upstream compartments includes two DN 16 CF flanges that enclose the sample assembly as illustrated in Fig. 1a. In this configuration, the copper disc carrying a freestanding membrane plays a role of a gasket that seals the flanges and has no direct contact with anything else. The heat conductor represents an L-shaped copper block of around 0.5 kg in weight and is equipped with a circular opening for mounting onto the membrane cell. Fig. 1b shows the heat conductor tightly clamped on the downstream flange to ensure

greater temperature changes in the sample compared to the walls of the feed compartment. This is because the heat transfer between the flanges occurs through the copper disc.

Two chromel–alumel thermocouples were used to monitor the membrane temperature with the help of a digital thermometer Voltcraft. One sensor was placed on the heat conductor near the cell, while the second one was placed into the side groove between the flanges. The latter reading was assumed to be the most appropriate estimate for the sample temperature although the two measurements differed little. During the operation, the membrane cell and the head of the heat conductor were wrapped with a polyethylene foam Mantel in order to provide thermal isolation and prevent frosting (Fig. 1c). A Dewar with liquid nitrogen and a hot water bath were employed to affect the tail of the heat conductor and thereby the temperature of the membrane cell. The newly designed experiment allows for the simultaneous recording of the feed pressure, the sample temperature, and the QMS output as a function of time. As the current in the QMS is proportional to the partial pressure of permeating molecules, the resulting $p–T–I$ data are a convenient way to show how the transmembrane flow rate changes with temperature at a given concentration gradient.

The preparation of CNMs from self-assembled biphenyl-4-carboxylic acid (TCI) by electron irradiation is detailed elsewhere.[23] The material is known to preserve a highly uniform thickness of around 1 nm with a sponge-like morphology. The areal pore density is estimated to be over 10^{13} cm^{-2}, and the pore diameter varies between 0.4 and 1.0 nm.[25] The membrane was transferred onto a silicon nitride window with
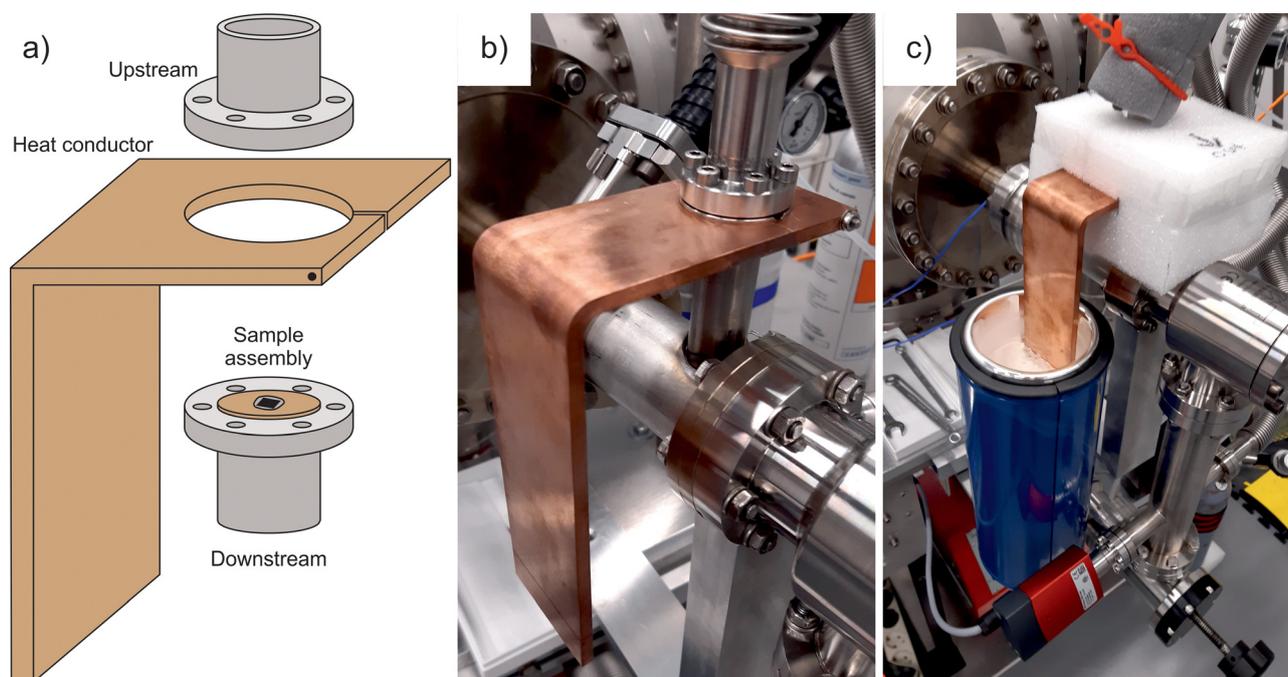
Fig. 1 (a) Schematic of the heat conductor and the membrane cell consisting of two flanges. The sample assembly is a copper disc glued to a silicon chip with a suspended membrane. (b) Photograph of the membrane cell with the heat conductor mounted on the downstream flange. (c) Photograph of the heat conductor in operation with its free end immersed into liquid nitrogen.

6950 | *Phys. Chem. Chem. Phys.*, 2024, **26**, 6949–6955

This journal is © the Owner Societies 2024

a 5 μm aperture (Silson Ltd) and fixed on the copper disc with epoxy glue (UHU Plus Endfest 300). After system evacuation, a leak test with helium was performed to prove intactness of the membrane. The permeation measurements were conducted at 2.0×10^{-9} mbar base pressure in the detection chamber. Heavy water (Sigma-Aldrich) was repeatedly degassed before experiments; ammonia (Linde) and isobutylene (Messer) were used as obtained.

Results and discussion

Fig. 2 illustrates the results of temperature-varied permeation measurements with vaporous heavy water. The mass spectrometer was set to detect D_2O^+ ions ($m/z = 20$), and the room temperature was 22 °C. In the beginning, the upstream compartment was connected to a turbomolecular pump; therefore,

Fig. 2 $p–T–I$ data for permeation of heavy water in CNMs. The blue curve is the feed pressure; the red curve is the membrane temperature; the black curve is the baseline-corrected QMS current.

the QMS signal was at the constant background level. Then, we allow water vapour to a reference nanoaperture in order to calibrate the detector as described previously.[18] This can be tracked by the synchronous signals in the pressure and the QMS output between 5 and 10 min that disappeared as soon as the gas molecules were pumped out. Starting from 18 min, the membrane was gradually fed with D_2O, and permeation caused the rise in the QMS signal. The container with the liquid was closed at 29 min when the pressure reached 14 mbar; at this point, the transmembrane flow entered a steady-state regime. The feed pressure slightly decreased due to adsorption on the walls of the feed chamber but stabilized above 13 mbar. The effective permeation rate was equal to 1.2×10^{-4} mol s^{-1} m^{-2} Pa^{-1} in the time interval from 30 to 34 min.

We began warming the heat conductor at 34 min which resulted in the rapid temperature increase in the membrane cell. For thermally activated processes, the temperature dependence of the rate constant k is described by the Arrhenius equation:

$$k = A\mathrm{e}^{-\frac{E_a}{RT}} \tag{1}$$

where A is the pre-exponential factor, E_a is the activation energy, T is the temperature and R is the gas constant. This relationship suggests the processes to accelerate with temperature, but Fig. 2 evidences that the QMS signal immediately dropped with heating despite a constant pressure in the upstream compartment. This means that much fewer D_2O molecules were passing through the membrane while their concentration remained the same. The stark anti-Arrhenius behaviour of the permeation rate is explained by the mechanism in which water vapour passes through CNMs *via* adsorption on the surface.[16–18] The difference in the shape of the QMS and pressure curves when D_2O was first supplied to the membrane was noted. The transmembrane flux grew non-linearly with the feed pressure which reflected the build-up of the adsorbed phase. The initial delay and acceleration at higher pressures agree with our prior kinetic modelling that suggests development from individual passage to cooperative motion.[18] It is the relative pressure that determines the extent of vapour condensation, and the membrane heating effectively gives rise to its local reduction. Desorption is likely to break down the single-file transport of hydrogen-bonded water molecules, but permeation of separate adsorbates appears feasible.[18]

Our experimental arrangement does not allow for establishing equilibria at different temperatures because employing the heat conductor longer would induce slow warming of the entire vacuum system. As soon as the sample temperature reached +50 °C, we reversed the process with the help of liquid nitrogen. From 40 to 45 min, the temperature quickly went down and was later brought to almost the ambient value by a bath of tap water. One can see that permeation of water molecules reacted swiftly to the cooling and the transmembrane flux also came back. The change in the membrane temperature seems to restore the surface coverage of adsorbed molecules even though the gas pressure was unaltered. The QMS signal at 50 min was
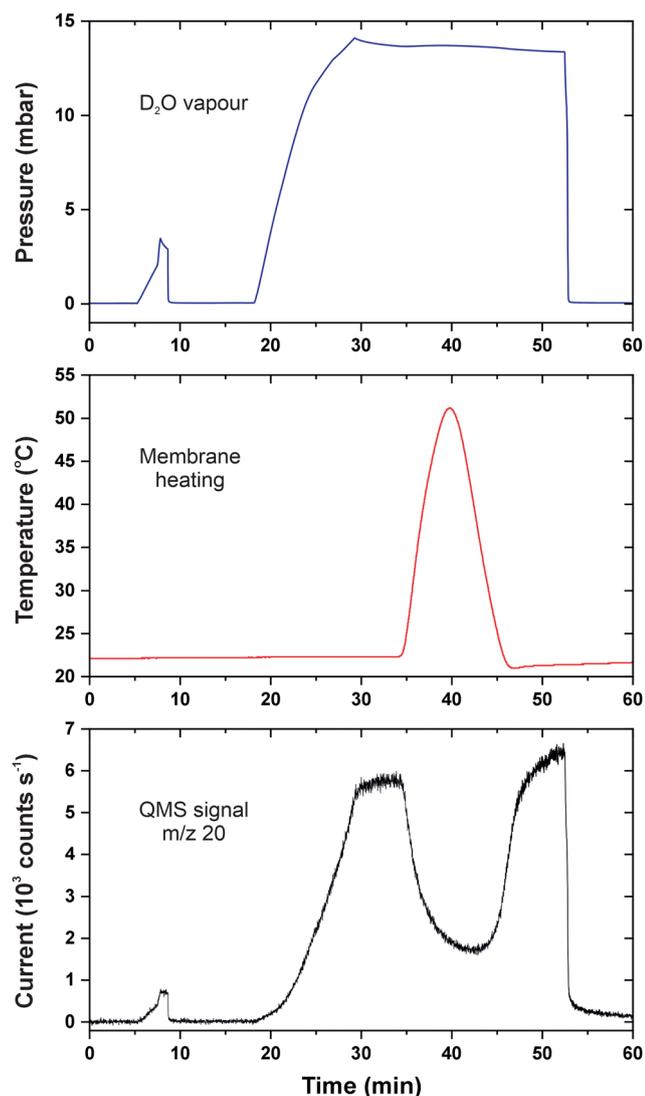
This journal is © the Owner Societies 2024

Phys. Chem. Chem. Phys., 2024, **26**, 6949–6955 | **6951**

somewhat higher than that at 30 min which is explained by the lower temperature and accumulation of D_2O in the detection chamber. At 53 min, the feed compartment was evacuated which led to the abrupt and simultaneous fall in the pressure and the number of permeating species. It follows that the surface-mediated flow across 2D membranes depends on pressure and temperature in line with gas adsorption isobars and isotherms.

In contrast to water that has a normal boiling point of +100 °C (nearly the same for heavy water), physisorption of inert gases is unfavourable at room temperature. The fact that nitrogen, argon, and oxygen cannot permeate through CNMs is consistent with their normal boiling points of −196, −186, and −183 °C, respectively.[26] To demonstrate the role of temperature on permeation of ordinary gases, we selected ammonia with a normal boiling point of −33 °C and molecular dimensions resembling water.[27] Fig. 3 shows the p–T–I data obtained with ammonia upon cooling the membrane cell with liquid nitrogen. The initial QMS signal corresponded to the residual concentration of particles with m/z = 17, and the upstream side was under vacuum. Again, detector calibration was first performed upon supplying 3 mbar ammonia to the reference nanoaperture which can be tracked by the small signal at around 7 min. Unlike Fig. 2, the corresponding signal at the pressure curve is barely seen because the scale spans a much greater range. From 18 to 25 min, the feed compartment was filled with ammonia up to 440 mbar which had virtually no impact on the QMS signal, *i.e.* the permeation of NH_3 molecules through CNMs was hindered.

For the steady-state mode (25–30 min), the ammonia permeance was calculated to be 3.8×10^{-8} mol s^{-1} m^{-2} Pa^{-1} which was practically at the limit of detection. The result is analogous to those obtained with other regular gases under similar pressure differentials. This is not surprising given the saturation vapour pressure of ammonia at room temperature was about 8.5 bar which translates the experimental parameters into the relative pressure of just 0.05. After 30 min, the membrane was rapidly cooled down below −30 °C, and the relative pressure in proximity of its surface increased accordingly. Contradictory to eqn (1), the data in Fig. 3 clearly show a sudden start of ammonia permeation around 43 min with the QMS signal going upward almost vertically. When the temperature turned to the opposite direction at 46 min, the flow rate of NH_3 molecules crossing the membrane fell instantly as well. The cooling was accompanied by a small decline in the upstream pressure indicating gas condensation on the walls of the membrane cell. The feed compartment was emptied at 62 min once the ambient temperature was regained.

Fig. 4 illustrates the permeation mechanism and highlights the difference between non-adsorbing and condensing species. For non-adsorbing particles, the probability of entering nanoscopic pores of comparable sizes is predicted to be low because of the repulsion by the atoms comprising the membrane.[28] At lower temperatures though, van der Waals attractions are favoured between the molecules and the membrane surface thus making the adsorbates pass into the pores much easier. In
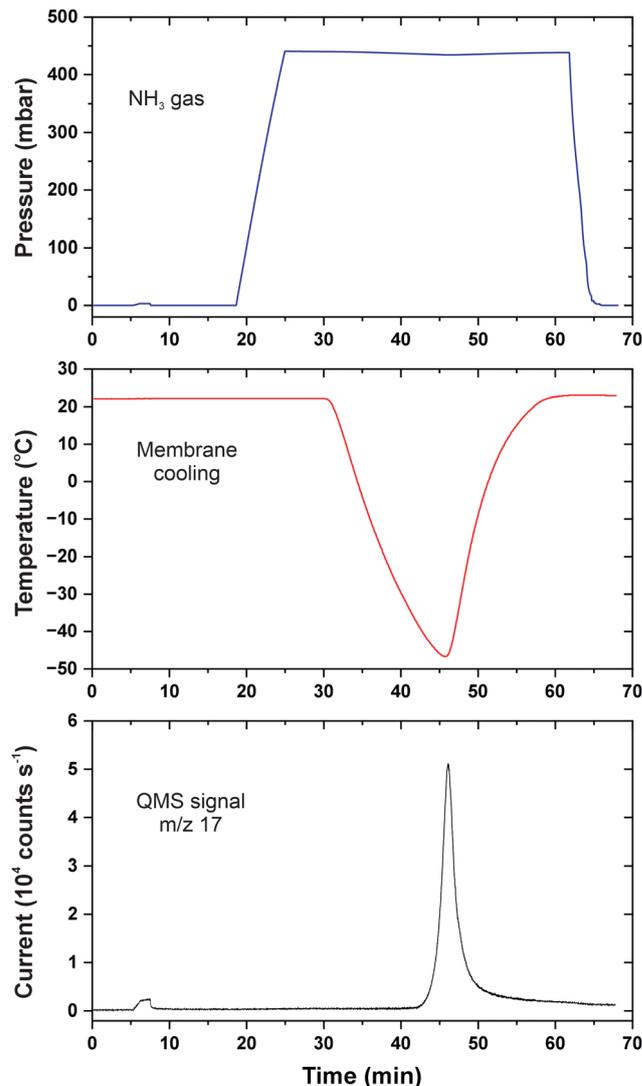

Fig. 3 p–T–I data for permeation of ammonia in CNMs. The blue curve is the feed pressure; the red curve is the membrane temperature; the black curve is the baseline-corrected QMS current.

terms of eqn (1), this can be considered as an effective increase of the pre-exponential factor for the net permeation rate. One can alternatively break down the process into two steps and express the permeation rate as a function of the adsorbate surface coverage.[18] Then, it becomes straightforward that cooling turns on the permeation by promoting physical adsorption and condensation.

The influx of ammonia into the detection chamber was so intense that the pressure was increased to 2.7×10^{-9} mbar. Like during the heating experiments, it was only reasonable to cool the cell transiently in order not to affect other parts of the setup; besides, the stability of the sample fixture was not tested below −50 °C. When the process was reversed, the peak permeation rate amounted to 1.2×10^{-5} mol s^{-1} m^{-2} Pa^{-1}, and compared to the permeance of water vapour, there was probably much room for further increase. The sharp kinetics is reminiscent of zero-order curves in temperature programmed
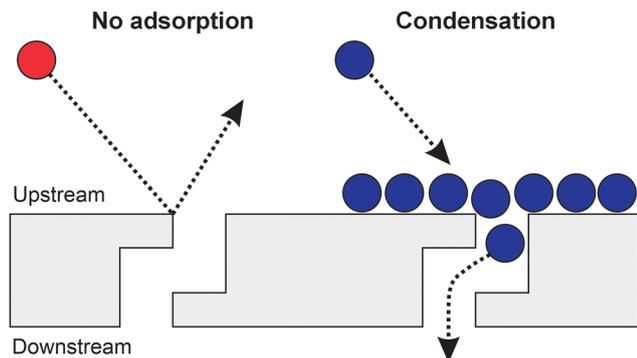
6952 | *Phys. Chem. Chem. Phys.*, 2024, **26**, 6949–6955

This journal is © the Owner Societies 2024

Fig. 4 Schematic of the gas permeation mechanism in CNMs. The red ball represents a non-adsorbing molecule that is backscattered upon impingement on the membrane surface. The blue balls depict condensing molecules that have a great likelihood to pass through the membrane pores.

desorption (TPD) which is the characteristic to phase transitions and implies the applicability of the Clausius–Clapeyron relationship.[29] We also conducted the experiment with NH_3 at an increased feed pressure of 490 mbar and plotted the resulting isobars as the transmembrane flux *versus* temperature (Fig. 5). As evident, there is a noticeable shift of the onset of permeation to higher temperatures which directly relates it to adsorption–desorption equilibria. This representation allows for extracting the temperature values T_1 and T_2 that yield the same flux at different gas pressures. The p_1, T_1 and p_2, T_2 pairs obtained can now be plugged to the approximate solution as follows:

$$\ln\frac{p_2}{p_1} \cong \frac{Q}{R}\left(\frac{1}{T_1} - \frac{1}{T_2}\right) \tag{2}$$

where Q is the latent heat and R is the gas constant. The results of the analysis are shown as a function of the flux in the inset of

Fig. 5 revealing an interesting trend. The latent heat appears to change with the flux similarly to the isosteric heat of adsorption confirming that the permeation is caused by physisorbed molecules. The flux emerges at low surface coverage of adsorbates when the heat amounts to around 34 kJ mol^{-1}, *i.e.* the adsorption energy of ammonia on CNMs. As more molecules get adsorbed, the flux increases and eventually goes up steeply. This leads to a decrease in the latent heat to 22 kJ mol^{-1} that matches well the enthalpy of vaporization for ammonia equal to 23.5 kJ mol^{-1}.[30] Thus, the anti-Arrhenius permeation is caused by non-activated physisorption and condensation.

This evaluation evidences that gas permeation in 2D membranes is sensitive to the presence of condensed molecules as long as their size fits the pores dimensions. Fig. 6 shows our next experiment with isobutylene that boils at −7 °C and liquefies easier than ammonia.[31] Its saturation pressure does not exceed 3 bar at room temperature, but the molecules are bulky and
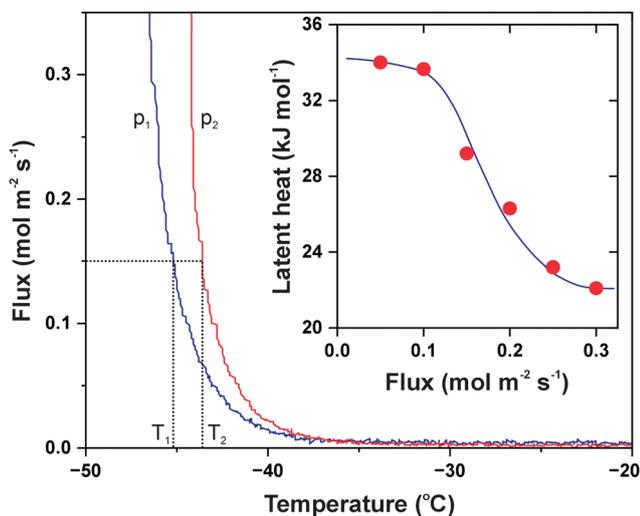

Fig. 5 Transmembrane flux of ammonia as a function of temperature measured at different feed pressures. The blue curve is for pressure p_1 = 440 mbar, and the red curve is for pressure p_2 = 490 mbar. The dotted lines illustrate temperature values for a given flux. The inset shows the results of the Clausius–Clapeyron analysis as a function of flux. The solid line is a guide for the eye.
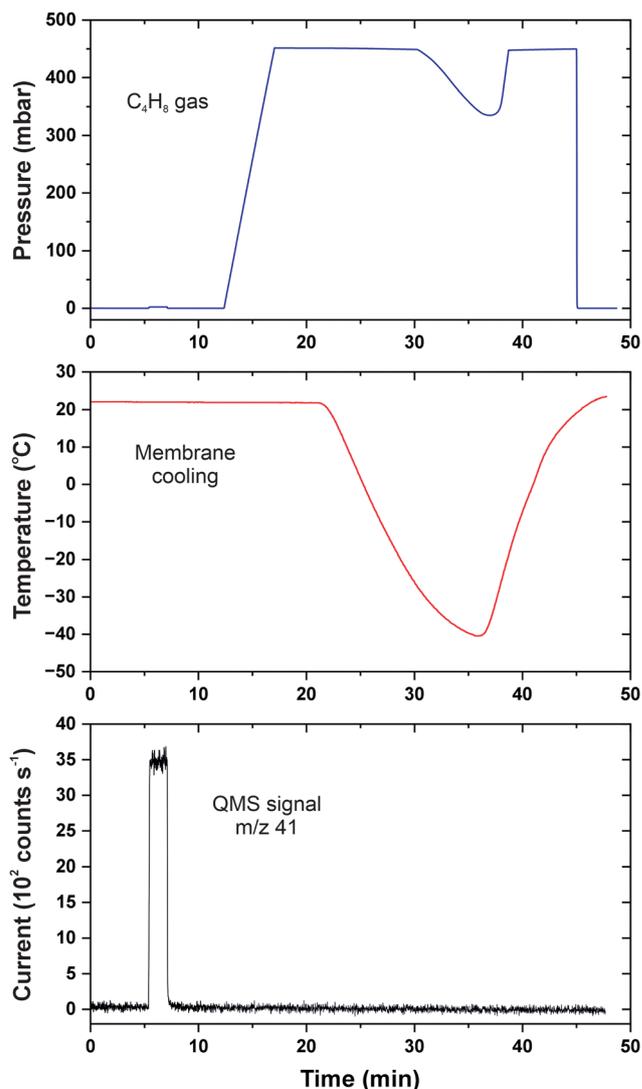

Fig. 6 p–T–I data for permeation of isobutylene in CNMs. The blue curve is the feed pressure; the red curve is the membrane temperature; the black curve is the baseline-corrected QMS current.

This journal is © the Owner Societies 2024

Phys. Chem. Chem. Phys., 2024, **26**, 6949–6955 | **6953**

hydrophobic. The detector was counting $C_3H_5^+$ ions (m/z = 41) when the calibration was done with 2.5 mbar isobutylene dosed to the reference nanoaperture between 6 and 7 min. The respective pressure rise appears very small with regard to the scale because 450 mbar of the gas was subsequently applied to the CNM. The steady-state mode between 17 and 21 min revealed no permeation of isobutylene which was followed by cooling the heat conductor with liquid nitrogen. The membrane temperature was decreased to −40 °C making the pressure decrease to 335 mbar; the feed pressure recovered with warming and vanished upon pumping at 45 min. The reversible pressure change clearly revealed massive condensation of C_4H_8 molecules in the membrane cell forming droplets or a thin layer. Nevertheless, the transmembrane flux remained negligible regardless of the temperature which was likely associated with the sieving properties of CNMs. It is known from prior studies that the interior of tortuous pores in the membrane is narrower in dimensions than their surface appearance.[32] It is also possible though that the liquefied hydrocarbon molecules were residing away from the hydrophilic CNM surface.

Recently, Stroganov *et al.* reported on gas transport experiments with morphologically similar CNMs and also observed the anti-Arrhenius behaviour of water vapour.[33] They measured the permeation rate of D_2O molecules as a function of pressure at 23, 41, 60 and 81 °C, and the heating appeared to slow down the transmembrane flow, especially when the membrane was exposed to the saturated vapour. The data plotted as a logarithm of the permeance *versus* reciprocal of the temperature revealed non-linear curves with negative values of the apparent activation energy. Thermodynamic estimates agreed well with the enthalpy of water adsorption and confirmed the two-step permeation mechanism, *i.e.* adsorption on the membrane surface followed by diffusion through the pores.

Conclusions

We introduced a viable experimental approach for probing molecular permeation in 2D membranes at elevated and cryogenic temperatures. The devised heat conductor enables prompt cooling down to −50 °C and heating up to +50 °C, and the achieved working range is extendable in both directions. As a case study, inherently microporous CNMs were subjected to transport measurements with vaporous heavy water, ammonia and isobutylene under isobaric conditions. Membrane heating was found to diminish the permeation rate of heavy water which was consistent with the surface-mediated mechanism. The pronounced anti-Arrhenius behaviour underscored the fact that transmembrane passage was interfered by desorption. Furthermore, the flow rate of ammonia was enhanced by orders of magnitude upon cooling while thermodynamic analysis confirmed gas condensation on the membrane surface. It was also shown that narrow pores in CNMs did not transmit isobutylene molecules in spite of their facile liquefaction at low temperatures. Our work proves the importance of interfacial processes in permeation across 2D

membranes and justifies selectivity towards vapours over regular gases. The implication is that gas separation can be facilitated by tuning the number of adsorbates *via* temperature, pressure, and surface affinity.

Conflicts of interest

There are no conflicts to declare.

Acknowledgements

References

1 N. Kavokine, M.-L. Bocquet and L. Bocquet, *Nature*, 2022, **602**, 84; X. Yu, A. Principi, K.-J. Tielrooij, M. Bonn and N. Kavokine, *Nat. Nanotechnol.*, 2023, **18**, 898.

2 S. P. Koenig, L. Wang, J. Pellegrino and J. S. Bunch, *Nat. Nanotechnol.*, 2012, **7**, 728.

3 K. Celebi, J. Buchheim, R. M. Wyss, A. Droudian, P. Gasser, I. Shorubalko, J.-I. Kye, C. Lee and H. G. Park, *Science*, 2014, **344**, 289.

4 S. C. O'Hern, M. S. H. Boutilier, J.-C. Idrobo, Y. Song, J. Kong, T. Laoui, M. Atieh and R. Karnik, *Nano Lett.*, 2014, **14**, 1234.

5 S. P. Surwade, S. N. Smirnov, I. V. Vlassiouk, R. R. Unocic, G. M. Veith, S. Dai and S. M. Mahurin, *Nat. Nanotechnol.*, 2015, **10**, 459.

6 M. S. H. Boutilier, D. Jang, J.-C. Idrobo, P. R. Kidambi, N. G. Hadjiconstantinou and R. Karnik, *ACS Nano*, 2017, **11**, 5726.

7 Z. Yuan, J. D. Benck, Y. Eatmon, D. Blankschtein and M. S. Strano, *Nano Lett.*, 2018, **18**, 5057.

8 C. T. Nguyen and A. Beskok, *Phys. Chem. Chem. Phys.*, 2019, **21**, 9483.

9 K.-P. Schlichting and D. Poulikakos, *ACS Appl. Mater. Interfaces*, 2020, **12**, 36468.

10 M. Ghosh, L. Madauß, M. Schleberger, H. Lebius, A. Benyagoub, J. A. Wood and R. G. H. Lammertink, *Langmuir*, 2020, **36**, 7400.

11 P. Z. Sun, M. Yagmurcukardes, R. Zhang, W. J. Kuang, M. Lozada-Hidalgo, B. L. Liu, H.-M. Cheng, F. C. Wang, F. M. Peeters, I. V. Grigorieva and A. K. Geim, *Nat. Commun.*, 2021, **12**, 7170.

12 J. Liu, L. Jin, F. I. Allen, Y. Gao, P. Ci, F. Kang and J. Wu, *Nano Lett.*, 2021, **21**, 2183.

13 D. Hou, S. Zhang, X. Chen, R. Song, D. Zhang, A. Yao, J. Sun, W. Wang, L. Sun, B. Chen, Z. Liu and L. Wang, *ACS Appl. Mater. Interfaces*, 2021, **13**, 10328.

14 L. Wang, M. S. H. Boutilier, P. R. Kidambi, D. Jang, N. G. Hadjiconstantinou and R. Karnik, *Nat. Nanotechnol.*, 2017, **12**, 509.

15 L. W. Drahushuk and M. S. Strano, *Langmuir*, 2012, **28**, 16671; C. Sun, M. S. H. Boutilier, H. Au, P. Poesio, B. Bai, R. Karnik and N. G. Hadjiconstantinou, *Langmuir*, 2014, **30**, 675; A. Jana, D. S. Bergsman and J. C. Grossman, *Nanoscale Adv.*, 2021, **3**, 4502.

16 P. Dementyev, N. Khayya, J. Kreie and A. Gölzhäuser, *ChemPhysChem*, 2022, **23**, 72.

17 N. Khayya, A. Gölzhäuser and P. Dementyev, *Phys. Chem. Chem. Phys.*, 2022, **24**, 12563.

18 P. Dementyev, T. Wilke, D. Naberezhnyi, D. Emmrich and A. Gölzhäuser, *Phys. Chem. Chem. Phys.*, 2019, **21**, 15471.

19 D. Naberezhnyi, S.-W. Park, W. Li, M. Westphal, X. Feng, R. Dong and P. Dementyev, *Small*, 2021, **17**, 2104392.

20 D. Naberezhnyi, L. Mai, N. Doudin, I. Ennen, A. Hütten, E. I. Altman, A. Devi and P. Dementyev, *Nano Lett.*, 2022, **22**, 1287.

21 J. Schrier, *ACS Appl. Mater. Interfaces*, 2012, **4**, 3745.

22 G. He, S. Huang, L. F. Villalobos, J. Zhao, M. Mensi, E. Oveisi, M. Rezaei and K. V. Agrawal, *Energy Environ. Sci.*, 2019, **12**, 3305.

23 D. Naberezhnyi and P. Dementyev, *Phys. Chem. Chem. Phys.*, 2020, **22**, 9808; P. Dementyev, D. Naberezhnyi, M. Westphal, M. Buck and A. Gölzhäuser, *ChemPhysChem*, 2020, **21**, 1006.

24 W. Guo, S. M. Mahurin, R. R. Unocic, H. Luo and S. Dai, *Nano Lett.*, 2020, **20**, 7995.

25 Y. Yang, P. Dementyev, N. Biere, D. Emmrich, P. Stohmann, R. Korzetz, X. Zhang, A. Beyer, S. Koch, D. Anselmetti and A. Gölzhäuser, *ACS Nano*, 2018, **12**, 4695; Y. Yang, R. Hillmann, Y. Qi, R. Korzetz, N. Biere, D. Emmrich, M. Westphal, B. Büker, A. Hütten, A. Beyer, D. Anselmetti and A. Gölzhäuser, *Adv. Mater.*, 2020, **32**, 1907850.

26 R. F. Barron, *Cryogenic Systems*, Oxford University Press, New York, 2nd edn, 1985.

27 C. S. Cragoe, C. H. Meyers and C. S. Taylor, *J. Am. Chem. Soc.*, 1920, **42**, 206.

28 Z. Yuan, R. P. Misra, A. G. Rajan, M. S. Strano and D. Blankschtein, *ACS Nano*, 2019, **13**, 11809; A. Rodriguez, K.-P. Schlichting, D. Poulikakos and M. Hu, *ACS Appl. Mater. Interfaces*, 2021, **13**, 39701.

29 W. Weiss and W. Ranke, *Prog. Surf. Sci.*, 2002, **70**, 1.

30 J. S. Chickos and W. E. Acree, *J. Phys. Chem. Ref. Data*, 2003, **32**, 519.

31 A. B. Lamb and E. E. Roper, *J. Am. Chem. Soc.*, 1940, **62**, 806.

32 P. Dementyev, Y. Yang, M. Rezvova and A. Gölzhäuser, *J. Phys. Chem. Lett.*, 2020, **11**, 238.

33 V. Stroganov, D. Hüger, C. Neumann, T. Noethel, M. Steinert, U. Hübner and A. Turchanin, *Small*, 2023, **19**, 2300282.